Underwater hyperspectral classification of deep sea corals exposed to a toxic compound

Paul Anton Letnes[*1], Ingrid Myrnes Hansen[1], Lars Martin Sandvik Aas[1], Ingvar Eide[2], Ragnhild Pettersen[3], Luca Tassara[3], Justine Receveur[4], Stephane le Floch[4], Julien Guyomarch[4], Lionel Camus[3], Jenny Bytingsvik[3]

1 Ecotone AS, Havnegata 9, NO-7010 Trondheim, Norway
2 Statoil ASA, Research and Technology, NO-7005 Trondheim, Norway
3 Akvaplan-niva AS, Fram Centre, P.O. Box 6606 Langnes, NO-9296 Tromsø, Norway
4 Centre de documentation, de recherche et d'expérimentations sur les pollutions accidentelles des eaux, 715 rue Alain Colas, CS 41836, 29218 BREST CEDEX 2, France

* paul.anton.letnes@gmail.com

Abstract

Tropical corals are routinely monitored from satellite and aeroplane using remote sensing techniques, revealing the health of coral reefs. Notably, coral bleaching is continuously monitored using multi- or hyperspectral imagery from satellites and aeroplanes. For deep-water corals, however, no established remote sensing technique exists, and for this reason, much less is known about the status of their habitats over time. The purpose of the present work was to evaluate the use of underwater hyperspectral imaging to detect changes in health status of both orange and white color morphs of the coral species *L. pertusa*. In this study, we examine the feasibility of similar ecosystem health monitoring by the use of underwater hyperspectral imagery. A total of 66 coral samples were exposed to 2-methylnaphthalene concentrations from $0\,\mathrm{mg\,L^{-1}}$ to $3.5\,\mathrm{mg\,L^{-1}}$, resulting in corals of varying health condition. By use of a machine learning model for classification of reflectance spectra, we were able to classify exposed corals according to lethal concentration (LC) levels LC5 (5 % mortality) and LC25 (25 % mortality). This is a first step in developing a remote sensing technique able to assess environmental impact on deep-water coral habitats over larger areas underwater.

Introduction

Coral reefs are the foundation of many marine ecosystems. Corals are found across the world's ocean, in both shallow tropical and subtropical waters and in deep water. Deep-water corals thrive in cold, dark water at depths of up to 6000 m [1]. They have a cosmopolitan distribution, being particularly abundant in the North East Atlantic, and are for instance found off the coast of Norway and deep underwater in the Mediterranean Sea. In contrast to tropical corals, they are azooxanthellate, meaning that they do not have symbiotic life forms with dinoflagellates and hence do not require direct access to sun light [2]. *Lophelia pertusa (Scleractinia)* (Linneaeus 1758) is one of the most abundant reef forming scleractininan deep-water corals in cold and temperate regions, with main occurrences at depths ranging from 200 m to 1000 m [3, 4]. The species is found as two color morphs (orange and white) due to different pigment composition causing phenotype specific optical fingerprints [5, 6]. The reef framework

offers structural habitat for a variety of benthic species [2], including gorgonian corals, sponges, squat lobsters (*Munida sarsi*) and rosefish (*Sebastes viviparoius*) as well as economically important fish species such as atlantic cod (*Gadus morhua*), saithe (*Pollachius virens*), and cusk (*Brosme brosme*) [3, 7–9].

The coral reefs are in danger, primarily due to climate change and increased CO_2 levels [10]. Climate change and ocean acidification can result in coral bleaching, slower growth [11] and reproduction rates, and degraded reef structure [12]. The increased CO_2 levels can affect the ability of the coral to form its aragonite skeleton [13, 14]. Other chemical and physical stressors may also damage corals. The oil industry is moving northwards and many of the drilling areas coincide with habitats listed by the Convention for the Protection of the Marine Environment of the North-East Atlantic (OSPAR) as being potentially rare or declining, including the cold-water coral reefs and sponge grounds. Corals and sponges are slow growing [15], and their habitats are therefore regarded as vulnerable to the smothering effects from drill cuttings [16]. Coral colonies affected by the Deepwater Horizon oil spill have shown signs of stress and mortality [17, 18]. Mechanical damages from trawling vessels is also considered a threat to the reefs [3, 15].

The Norwegian environmental regulatory authorities have imposed requirements for detailed habitat and organism mapping prior to exploratory drilling, as well as post-drilling surveying to map the distribution of deposited drill cuttings and the extent of possible biological impacts. Further, mapping of sensitive species and habitats to accidental oil pollution is an essential part of contingency plans, and species distribution maps are a crucial tool to assist responders during an incident, especially when the industrial activities are near shore.

Hyperspectral imaging is widely used as an in situ and non-invasive sensor for species mapping and detection of ecosystem health status [19]. For instance, shallow water corals are monitored by remote sensing from satellites [20]. Hyperspectral imagers are typically deployed from satellite or aeroplane [21], however, underwater imaging using spectral signals have been used to measure changes in coral appearance [22–24]. Hyperspectral imaging collects and processes incoming light across a range of the optical spectrum. In contrast to ordinary photographic cameras (or similarly, the human eye) which record only three color bands (red, green, and blue), a hyperspectral camera produces a full spectrum of all available wavebands in each pixel in an image. Objects will reflect and absorb light to a varying degree at different wavelengths depending on their color and pigmentation providing a spectral signature of that object.

The Underwater Hyperspectral Imager (UHI) used in the present work represents a new system for identification, mapping and monitoring of objects of interest (OOI) at the seabed [25–27]. Underwater hyperspectral imaging is constrained to the visible part of the spectrum, as both ultra violet and infrared radiation is attenuated in water [28]. Hyperspectral imaging generates large amounts of data which require sophisticated data analysis and machine learning methods [29]. Multivariate data analysis and machine learning have been used successfully in several marine environmental studies for the interpretation of large data sets, for example in integrated environmental monitoring [30] and for the analyses of photos to assess the potential impact of water-based drill cuttings on deep-water rhodolith-forming calcareous algae [31].

The purpose of the present work was to evaluate the use of UHI and multivariate data analysis to detect changes in health condition of the coral species *L. pertusa*. Corals were exposed to 2-methylnaphthalene in laboratory experiments in order to provide corals with health condition varying from unaffected to dead. Hyperspectral images of exposed and control corals were then recorded after a recovery period. Finally, classification of these images using machine learning shows in a visual way which spatial areas are affected by exposure to toxic compounds.

Materials and methods

The experimental work presented in this study consists of the following activities: collecting and rearing coral samples, exposing the corals to the toxicant 2-methylnaphthalene, monitor corals to determine polyp mortality, and imaging the corals using UHI. An overview of the timeline is given in Table 1.

Table 1. Timeline of experimental activities.

Date	Time T (h)	Activity
2016-03-05	-24	Acclimatization start
2016-03-06	0	Exposure start
2016-03-10	96	Exposure end
2016-03-10	96	Recovery period start
2016-05-03	1392	UHI scanning of all coral samples
2016-05-03	1440	Classification of polyp mortality

Sampling and rearing of corals

Samples of *L. pertusa* were collected at Stokkbergneset in Trondheimsfjorden (Norway, 63.47°, 9.91°) on September 1st 2015 in collaboration with the Norwegian University of Science and Technology (NTNU) onboard R/V Gunnerus. The site is characterized by a steep rock wall with *L. pertusa* occurring in colonies from 100 m to 500 m depth [32]. The coral samples were collected from four different colonies and included both white and orange color morphs. A remotely operated vehicle (ROV) ("Minerva") with an attached fish net was used to conduct the sampling. The corals were transported to the Akvaplan-niva Research and Innovation Center Kraknes (RISK) (Tromsø, Norway) by car in a water tank where temperature, oxygen levels and oxygen saturation were frequently monitored. The temperature range and oxygen saturation during transport was 5.1 °C to 9.8 °C and 98 % to 113 %, respectively. The pieces of *L. pertusa* were divided into smaller samples (one sample refers to a coral branch with 3 to 9 polyps) and placed in silicon tubes placed in steel grids (20 cm × 40 cm) in 500 L tanks with a continuous flow (500 L h^{-1}) of filtered (60 µm filter) and UV-treated bottom sea water (63 m depth) from the fjord Sandøysundet, adjacent to the research facility. The temperature, oxygen saturation, and oxygen concentration were monitored on a daily basis during rearing, and the corals were fed three times per week with *Calanus* sp. naupli from Planktonic AS. The corals were cleaned from sediments once per week.

Exposure setup and procedure

The set-up comprised five treatment groups: one control group (C0) and four exposed groups (C1, C2, C3, and C4). Each treatment group consisted of four replicates (R1, R2, R3, and R4). Each replicate consisted of one orange and two white pigmented morphs, giving a total of 20 orange and 40 white coral samples. The corals were assessed to be in good condition when sampled. In addition, the samples were selected randomly to represent all four coral colonies at Stokkbergneset. Each sample comprised a coral branch with 3 to 9 polyps. Briefly, after 24 h acclimatization, *L. pertusa* were used in a 96 h acute toxicity testing to 2-methylnaphthalene (see Table 1 for a timeline). During acclimatization and exposure, each coral replicate were kept in a square glass aquarium containing 1.5 L sea water. The animals were not fed during the toxicity testing.

The acute toxicity tests to 2-methylnaphthalene involves passive dosing. Based on the method described by [33], a passive dosage system using silicone O-rings has been developed. This was done to obtain a stable concentration of 2-methylnaphthalene as close to the nominal concentration as possible. The O-rings were cleaned before they were loaded with 2-methylnaphthalene with target concentrations in seawater of $0\,\mathrm{mg\,L^{-1}}$, $1.03\,\mathrm{mg\,L^{-1}}$, $2.27\,\mathrm{mg\,L^{-1}}$, $5.00\,\mathrm{mg\,L^{-1}}$, and $8\,\mathrm{mg\,L^{-1}}$ to $10\,\mathrm{mg\,L^{-1}}$ (saturation) for C0 to C4, respectively. After O-rings were loaded, they were set to equilibrate with seawater in 20 L bottles for 24 h, one bottle per treatment group. The final stock solution was pumped into the exposure chambers continuously using a peristaltic pump with the inlet placed in the bottom of the exposure beakers as illustrated in Fig 1. Overflow ensured that the overhead between water surface and glass lids covering the exposure beakers always was at a minimum. Using O-rings combined with a pump is beneficial as it reduces the interference and stress on the corals during the exposure period. Based on a combination of the coral oxygen needs, chemistry and kinetics, tubing capacity, pump capacity and practical reasons, a flow rate of approximately $160\,\mathrm{mL\,h^{-1}}$ was selected. The exchange rate of exposure solvent in the exposure beakers was about 2.5 times per 24 h. In addition to logging of temperature every 30 min throughout the 96 h exposure (Tidbit Temperature Data Logger V2, Onset, Massachusetts), the temperature and oxygen saturation was measured daily throughout the experiment (Oxyguard). The chambers were covered with a glass lid to reduce evaporation of 2-methylnaphthalene. All stock solution bottles and treatment group replicates were placed on a magnet stirrer throughout the whole experiment to keep the exposure media homogeneous. The exposure was conducted in a room holding $4 \pm 1\,^{\circ}\mathrm{C}$. After the toxicity test was ended, all coral samples were kept for approximately 12 h in individual tanks with pure seawater to provide an initial period of depuration of 2-methylnaphthalene before they were transferred to a single recovery tank of the same type and with similar facilities as they were kept in prior to the toxicity test.

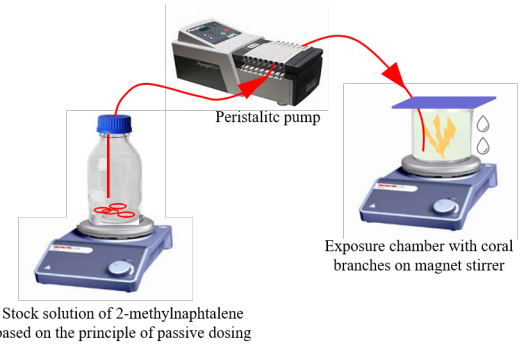

Fig 1. Setup for 2-methylnaphthalene exposure. A peristaltic pump circulates stock solution to the exposure chamber.

In addition to the five treatment groups, six coral samples (two orange and four white samples) referred to as reference alive were also selected. The reference alive corals represented samples from the same coral colonies as the samples used in the toxicity test. The reference samples were kept in the rearing tanks with pure seawater while the C0–C4 corals went through the toxicity experiment. Reference alive corals were kept in the same tank as C0–C4 during the recovery period. Hence, reference alive corals were exposed to minimal handling compared to C0–C4 before they were scanned by the UHI. The reference alive group was included as an additional control group in case of accidental contamination of the experimental control group (C0) or in case handling itself affected the corals and their spectral properties.

Polyp mortality

Prior to exposure to 2-methylnaphthalene (at time −24 h, see Table 1 for a timeline), the number of alive polyps on each coral samples were counted. Mortality was assessed after recovery and UHI scans (at time 1440 h). This approach was chosen because it was not possible to determine whether polyps were alive or dead immediately after exposure was ended. By keeping the coral samples in a recovery tank over weeks the samples and individual polyps could be monitored visually for the presence of soft tissue on skeleton and polyps. A polyp was classified as dead when soft tissue was no longer present within the polyp's calyx. Illustration of live and dead polyps are given in Figure 2. The fraction of dead polyps (i.e., the number of dead polyps divded by the number of alive polyps before toxicant exposure) is presented in results and statistics as polyp mortality.

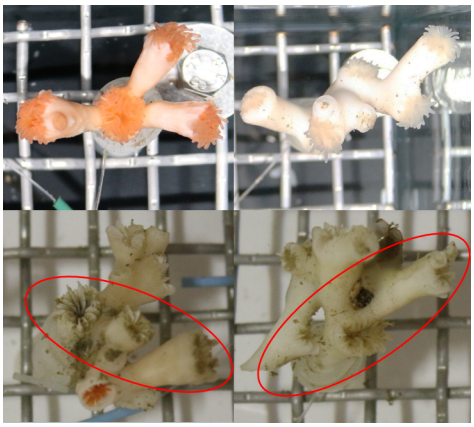

Fig 2. Example images of living and dead corals. Example images of alive and dead polyps. Top pictures from time 0 h: orange and white coral samples with healthy polyps. Lower pictures from time 1392 h: orange and white coral samples with dead polyps (red ellipse indicate dead polyps). The coral sample in the lower picture to the left was orange, but after exposure to 2-methylnaphthalene it lost pigments and pigmented tissue and turned white. The coral sample in the lower picture to the right show a white coral sample with dead polyps

Chemical analysis of exposure concentration

Preparation of water samples

10 mL water samples were collected from the exposure beakers in Tromsø, Norway. Samples were acidified to pH 1 using hydrogen chloride (HCl), added methanolic solution (1.8 mL) of perdeuterated naphthalene (Nd8) at the concentration of 100 µg mL^{-1} and frozen at −20 °C. The final concentration of Nd8 in water samples was 15.3 µg mL^{-1}. The water samples were then sent to Brest, France in a cool box for analysis.

Extraction of water samples and conditions of analysis

The water samples were thawed overnight in the fridge, and then extracted with 2 mL of pentane. A calibration curve was established for 2-methylnaphthalene concentrations in the range 0 mg L^{-1} to 10 mg L^{-1} with a fixed concentration of Nd8.

Samples were analyzed by Gas Chromatography coupled to Mass Spectrometry (GC-MS). The GC was an HP 7890 series II (Hewlett-Packard. Palo Alto. CA. USA) equipped with a Multi Mode Injector (MMI) used in the pulsed splitless mode (Pulse

Splitless time: 1 min. Pulse Pressure: 103 kPa). The injector temperature was maintained at 300 °C and 1 µL of the extract was injected. The interface temperature was 300 °C. The GC temperature gradient was from 70 °C (0 min) to 250 °C (0 min) at 15 °C min^{-1}. The carrier gas was Helium at a constant flow of 1 mL min^{-1}. The capillary column used was a HP 5-ms (Hewlett–Packard, Palo Alto. CA. USA, 30 m in length, 0.25 mm internal diameter, and a film thickness of 0.25 µm). The GC was coupled to a HP 5975 Mass Selective Detector (MSD) used in the Electronic Impact mode (electronic impact energy 70 eV, system temperatures: 230 °C (source) and 150 °C (quadrupole)). 2-methylnaphthalene quantifications were done using Single Ion Monitoring mode with respectively the molecular ion of each compound at a minimum rate of 2 s^{-1} (mass/charge ratio of 142 for 2-methylnaphthalene and 136 for Nd8). 2-methylnaphthalene was quantified relatively to the perdeuterated Nd8 introduced at the beginning of the sample preparation procedure using calibration curves.

Underwater hyperspectral imaging

The underwater hyperspectral imager is a line camera (sometimes referred to as a "push broom" sensor), consisting of a thin slit, a spectrograph, and a monochrome camera, mounted in a waterproof housing. For capturing area images, it is installed on a moving platform, where it captures frames perpendicular to its direction of flight. The camera system acquires information about the incoming light at wavelengths from 381 nm to 846 nm.

Coral samples and reflectance references were placed in a tank of dimensions 2.0 m × 1.0 m × 1.6 m, filled with sea water. The UHI and lighting was mounted on a linear motorized rail; see Fig 3. The vertical distance between the spectrograph and coral samples was 0.35 m. Two halogen lamps (Osram Decostar 51 TITAN 50 W 12 V 60° GU5.3) with constant power supply were the only light sources during the measurements. Halogen lights were used because of their relative good uniformity across the wavelengths of light for which water is transparent. The whole setup was surrounded by a black tent to avoid light pollution. The UHI was moved along the rail with a constant speed of (0.13 m s^{-1}) during imaging. The spatial resolution of the recorded images was approximately 2.5 mm and the diffraction limited spectral resolution was approximately 5 nm, while the spectra were sampled approximately every 0.5 nm.

Reflectance conversion

Following data acquisition, the hyperspectral images were converted to optical reflectance images. This is necessary in order to correct for the wavelength and optical path length dependent attenuation of water. This was done based on direct measurement of a Spectralon (Labsphere inc), a diffuse reflectance standard, with dimensions 20 cm × 20 cm × 3 cm. The coral samples were estimated to have a height of 7 cm. In order to correct for their height, an inclined PVC plate was introduced covering the full field of view of the UHI.

By comparing the measured spectra of the Spectralon, $I_{\mathrm{spec}}(x, \lambda)$, with its calibrated reflectance spectrum, $R_{\mathrm{spec}}(\lambda)$, a conversion factor, $A(x, \lambda)$, was found for every spatial pixel (at position x) covered by the Spectralon.

$$A_{\mathrm{spec}}(x, \lambda) = \frac{I_{\mathrm{spec}}(x, \lambda)}{R_{\mathrm{spec}}(\lambda)} \tag{1}$$

The reflectance of the PVC, $R_{\mathrm{PVC}}(\lambda)$, was then calculated by applying the conversion factor, $A_{\mathrm{spec}}(x, \lambda)$, to the spatial pixels in the UHI slit covering the Spectralon, when

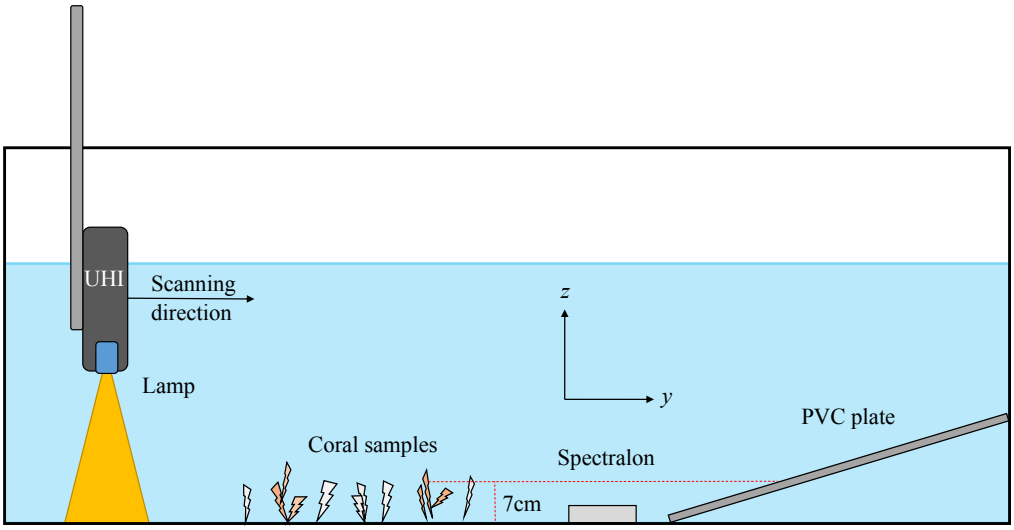

Fig 3. Experimental setup for UHI image acquisition. Samples of *L. pertusa* were set up on the bottom of a tank and imaged using an underwater hyperspectral imager (UHI). The UHI was attached to a linear scanning mechanism and operated in a "push-broom" fashion. The setup also includes a Spectralon reference plate and an inclined reference plate to account for changes in the spectrum due to the presence of water.

imaging the PVC at 3 cm:

$$R_{\mathrm{PVC}}(\lambda) = \sum_x \frac{I_{\mathrm{PVC}}(x, z = 3\mathrm{cm}, \lambda)}{N_{\mathrm{spec}} A_{\mathrm{spec}}(x, \lambda)} \tag{2}$$

Finally, conversion factors could then be found for all spatial pixels in the slit at any altitude,

$$A(x, z, \lambda) = \frac{I_{\mathrm{PVC}}(x, z, \lambda)}{R_{\mathrm{PVC}}(\lambda)}, \tag{3}$$

and be applied to acquire the reflectance at the altitude of the corals for the full image:

$$R(x, y, z = 7\mathrm{cm}, \lambda) = \frac{I(x, y, \lambda)}{A(x, z = 7\mathrm{cm}, \lambda)}. \tag{4}$$

where $I(x, y, \lambda)$ is the recorded intensity, i.e., the hyperspectral image.

Pixel extraction

The reflectance spectra from each coral sample was extracted by manually selecting image pixels; a total of 103 to 718 pixels were selected depending on the size of the coral. Pixels were selected both from the branches and the polyps of the coral. The reflectance spectrum was labelled with the sample ID and stored as an entry in a database. Each entry contained information about the normalized reflectance for each pixel at each wavelength from 381 nm to 846 nm, and the pixel position in the original UHI image (corresponding to the position in the tank).

Data used in spectral classification

Spectra were recorded for 60 coral samples representing the C0 to C4 corals used in the exposure study, as well as for the 6 reference alive corals. Due to poor transmission of

ultra violet and near infrared wavelengths even in extremely clean water [28], poor signal quality was experienced in both ends of the spectrum. Therefore, only data from the spectral range 400 nm to 750 nm are included in this study. The spectra recorded are placed in a matrix $\mathbf{X}$, where each column corresponds to one wavelength, and each row corresponds to one observation, i.e., a pixel in the hyperspectral image.

The matrix $\mathbf{Y}_h$, used for Projection to Latent Structures (PLS) [34] in the *preprocessing* stage only, consists of the following columns: 2-methylnaphthalene concentration and polyp mortality. Each row of the matrix $\mathbf{Y}_h$ corresponds to the same row in $\mathbf{X}$, i.e., spectra associated with the same coral sample.

The vector $\mathbf{Y}_c$, used for *classification*, consists of one categorical variable, namely, the exposure category of the organism which the spectrum came from. The exposure category is determined by the LC5 and LC25 concentration (lethal concentration for 5 % and 25 % of polyps) of 2-methylnaphthalene: the *non- or low* exposure category was exposed to a concentration $C \leq \text{LC5}$; the *intermediate* exposure category was exposed with $\text{LC5} < C \leq \text{LC25}$; and the *high* exposure category was exposed with $C > \text{LC25}$.

Classification algorithm

A three-stage machine learning model was applied to classify the exposure level of the coral samples. An overview of the data analysis process is given in Fig 4, showing the ordering of including reflectance conversion of the image, extraction of image pixels into a database, and classification model. In all cases, separate models were trained on spectra from white and orange corals, as the pigmentation of the coral can easily be determined using a simple linear classifier.

The stages consist of standardization, PLS and transformation, followed by an ν-Support Vector Machine (νSVM) classification algorithm [35–37]. Note that linear classification algorithms were found to be unsuitable to the problem at hand, due to to the nonlinear separation of points in the PLS latent variable space. The `scikit-learn` software package was used for both of the PLS and SVM algorithms [35].

Standardization of spectra

Before attempting classification, the model inputs were standardized:

$$z_i = \frac{x_i - \mu_i}{\sigma_i} \tag{5}$$

where z_i is the scaled value, x_i is the original value, and μ_i and σ_i is the mean and standard deviation of feature i (i.e., the spectrum intensity at wavelength i), respectively. Following standardization, all input variables to the model have zero mean and unit variance. This avoids the problem of some variables being weighted more heavily due to, e.g., different units: the importance of a variable should not depend on whether it is measured in milligram or kilogram. Each feature corresponds to a wavelength in the spectrum, and a column of the input data matrix X:

$$\mathbf{X} = [x_1 x_2 \dots x_i \dots] \tag{6}$$

where the x_i are column vectors containing all measurement values. Similarly, standardization was also performed on $\mathbf{Y}_h$ (2-methylnaphthalene concentration and polyp mortality).

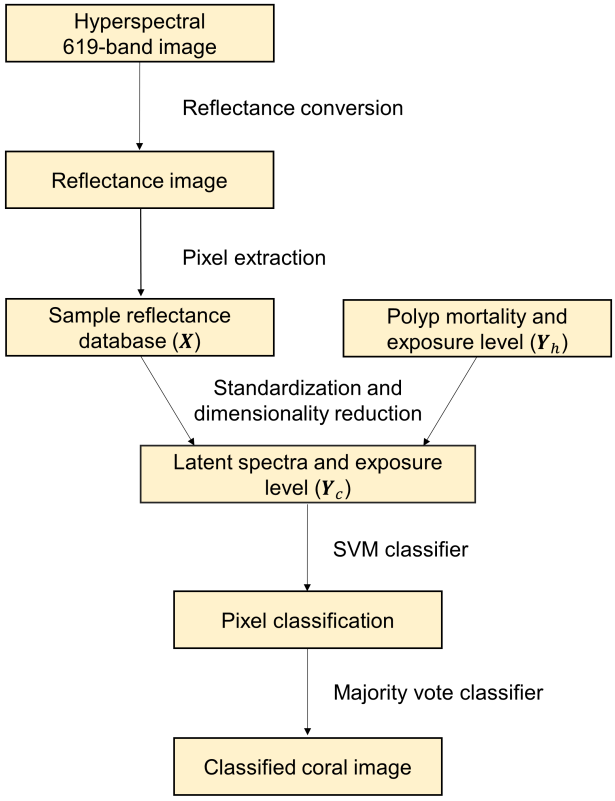

Fig 4. Data analysis flowchart. The flowchart shows the full data analysis pipeline including all steps of the classification model.

Dimensionality reduction

Following standardization of inputs, a PLS model relating spectra ($\mathbf{X}$) to 2-methylnaphthalene concentration and polyp mortality ($\mathbf{Y}_h$) is constructed:

$$\mathbf{Y}_h = \mathbf{B}\mathbf{X} + \mathbf{E} \tag{7}$$

where $\mathbf{E}$ is the error term. In the process of constructing the regression coefficient matrix, $\mathbf{B}$, the input matrix $\mathbf{X}$ is transformed to a lower-dimensional (latent) subspace; hence, the name PLS. This is done in a way such that the covariance between the $\mathbf{X}$ and $\mathbf{Y}_h$ matrices is maximized. Furthermore, PLS selects variables that extract the maximum relevant information possible. These *latent variables* are simply weighted sums of the original variables (e.g., the recorded spectrum intensity at each wavelength). One can think of the colors red, green, and blue as three latent variables used by our eyes to interpret the optical spectrum. The vector of the weights are referred to as *loading vectors* and reveals which underlying variables (in our case, wavelengths) that have the most explanatory power. Note that the loadings are ordered such that the first PLS component contains the most explanatory power, and subsequent component contain less and less explanatory power between the variables. In our case, a

dimensionality reduction from 619 dimensions (wavelengths) to 10 dimensions (i.e., 10 latent variables) was chosen. The number of latent variables was selected using 5-fold stratified cross-validation [38]; however, we note that the results were not sensitive to the exact number of latent variables, and that classification performed well for 5 to 20 latent variables.

Subsequently, classification is improved both in quality and speed, as noise is removed and the dimensionality of input data is reduced significantly. Also, separation of spectra is improved as the PLS algorithm maximizes covariance between spectra and 2-methylnaphthalene concentration and polyp mortality.

Classification of spectra and samples

The input to the classification stage is, as described above, spectra ($\mathbf{X}$) transformed into the 10-dimensional PLS latent variable space, as well as 2-methylnaphthalene concentration and polyp mortality ($\mathbf{Y}_c$). The νSVM model constructed uses the parameter $\nu = 0.1$ and a radial basis function kernel [36], as the spectra are not linearly separable in the latent variable space.

After classification of individual spectra, we classify each coral sample to the class with the highest number of single spectra (the majority vote algorithm). This lends significant robustness to incorrect classification, as many individual spectra can be classified incorrectly without affecting overall area coverage.

We note that model training and testing takes on the order of one minute on a desktop computer, and the use of the model to classify new data require only fast and well optimized computational operations, e.g., matrix multiplication. As such, the computational requirements are light, and should not pose any problems for practical use.

Results and discussion

Chemical analysis of 2-methylnaphthalene concentration

Chemical analysis of water samples from the stock bottles confirm that the desired concentrations of 2-methylnaphthalene, by using loaded silicon O-rings, were obtained. The average 2-methylnaphthalene concentration in the water samples from the stock bottles sampled at time 0 h, 24 h, 48 h, and 72 h were 125 %, 115 %, 70 %, and 98 % of nominal concentrations for C1 to C4, respectively (see Table 2 and S1 Table: Measured 2-methylnaphthalene concentration in stock bottles and exposure beakers). The 2-methylnaphthalene levels in the C0 stock bottles samples at the same time points were all below $0.033\,\mathrm{mg\,L^{-1}}$ (which was the limit of detection), and hence, regarded as acceptable. The 2-methylnaphthalene concentration in the water samples from the exposure beakers sampled from T0 to T72 were somewhat lower than in the stock bottles with C1 to C4 calculated to be 43 % (replicates ranging from 38 % to 51 %), 47 % (replicates ranging from 40 % to 60 %), 27 % (replicates ranging from 2 % to 47 %) and 32 % (replicates ranging from 26 % to 42 %) of nominal concentrations, respectively; see Table 2 and S1 Table: Measured 2-methylnaphthalene concentration in stock bottles and exposure beakers. However, one of the four C3 replicates (R2) deviated from the others. The replicate C3 R2 contained significantly lower 2-methylnaphthalene concentrations than the other replicates with only 2 % of nominal concentration achieved, while the remaining three replicates ranged from 39 % to 47 % of the nominal value (see S1 Table: Measured 2-methylnaphthalene concentration in stock bottles and exposure beakers). The deviation of C3 R2 was probably due to a faulty pump channel. The levels of 2-methylnaphthalene in the control (C0) beakers were all below

0.07 mg L^{-1}, and hence, regarded as acceptable. The lower concentration of 2-methylnaphthalene in the exposure beakers compared to the stock bottles is likely explained by evaporation of 2-methylnaphthalene from water masses to air as the systems were not completely closed. As stock solutions were pumped through the tubes connecting the stock bottle and the exposure beakers 24 h prior to exposure start, and as teflon coated tubes were used, we believe that there was no loss of 2-methylnaphthalene during the 96 h exposure period due to 2-methylnaphthalene sticking to the tube walls. It is unlikely that bioaccumulation of 2-methylnaphthalene in coral tissue was of significance as the biomass of corals in each replicate beaker was low (ranging from 9 g to 21 g coral, skeleton and soft tissue, in 1.5 L sea water). In all beakers, the concentration of 2-methylnaphthalene was lower at T0 than measured at later time points. This initial increase are explained by non-contaminated water masses being replaced by contaminated stock solution during the first hours (flow of approximately 160 mL h^{-1}) of the exposure period. Besides this, the concentration of 2-methylnaphthalene in the exposure beakers correlates with the concentrations in the stock solutions (Pearsons' correlation $R^2 = 0.61$, $p \leq 0.001$).

Table 2. Concentration of 2-methylnaphthalene (mg L^{-1})

Exposure group		C0	C1	C2	C3	C4
Nominal concentration (mg L^{-1})		0.0	1.0	2.3	5.0	8.0
Stock solution	avg	0.0	1.3	2.6	3.5	7.8
	std dev	0.0	0.2	0.5	1.3	1.2
	min	0.0	1.0	1.9	1.8	6.1
	max	0.0	1.5	3.2	5.0	10.2
Beakers 1–4 (avg)	avg	0.0	0.4	1.1	1.3	2.6
	std dev	0.0	0.2	0.6	1.7	1.4
	min	0.0	0.0	0.0	0.0	0.0
	max	0.1	0.8	2.0	8.9	4.9
Beaker 1	avg	0.0	0.4	1.4	1.4	2.6
	std dev	0.0	0.3	0.7	0.8	1.2
	min	0.0	0.0	0.4	0.4	1.0
	max	0.0	0.6	2.0	2.3	3.9
Beaker 2	avg	0.0	0.4	1.0	0.1	2.4
	std dev	0.0	0.2	0.4	0.2	1.6
	min	0.0	0.1	0.3	0.0	0.0
	max	0.0	0.7	1.3	0.5	4.2
Beaker 3	avg	0.0	0.4	1.0	2.4	3.4
	std dev	0.0	0.2	0.6	2.8	1.5
	min	0.0	0.1	0.0	0.4	1.0
	max	0.0	0.7	1.5	8.9	4.9
Beaker 4	avg	0.0	0.5	0.9	1.4	2.0
	std dev	0.0	0.3	0.6	0.9	1.4
	min	0.0	0.1	0.0	0.4	0.0
	max	0.1	0.8	1.4	2.7	3.5

Concentration of 2-methylnaphthalene (mg L^{-1}) measured in water samples collected from stock solutions and exposure beakers every 24 h in the 96 h exposure period. Concentrations are given as average (avg), standard deviation (std dev), minimum (min), and maximum (max) values based on measured concentration in duplicate water samples from each time points. Nominal concentrations are listed for each exposure group.

Polyp mortality

The fraction of dead polyps at the end of the experiment correlated with the 2-methylnaphthalene exposure doses, and based on the sigmoidal dose-response curve the LC5 and LC25 values were determined (Fig 5). Each point in the figure represent one sample (with 3 to 9 polyps), with groups of 3 samples sharing the same 2-methylnaphthalene concentration, as they were placed in the same exposure beaker. Concentrations of 2-methylnaphthalene are based on levels in water samples collected during the exposure period, while the polyp mortality was assessed approximately 8 weeks later. This approach was necessary because it was challenging, if not impossible, to determine whether polyps were alive or dead shortly after exposure was ended. The coral samples could have both live and dead polyps at the time they were assessed. Whether mortality of one single polyp have any impact on neighboring polyps are unknown as there to our knowledge is highly limited knowledge about communication and signaling between polyps of L. pertusa. However, it has been shown that there are no nervous communication between polyp in *L. pertusa* colonies [39]. Although no firm conclusion can be given, we believe that there has been no influence of intercommunication between polyps affecting our mortality data.

The variation in polyp mortality was relatively high with a polyp mortality ranging from 0 % to 50 % for concentrations from $0.9\,\mathrm{mg\,L^{-1}}$ to $2.3\,\mathrm{mg\,L^{-1}}$, and a polyp mortality ranging from 0 % to 100 % for concentrations between $2.3\,\mathrm{mg\,L^{-1}}$ to $2.7\,\mathrm{mg\,L^{-1}}$. The mortality ranged from 0 % to 17 % for concentrations of 2-methylnaphthalene ranging from $0.0\,\mathrm{mg\,L^{-1}}$ to $0.9\,\mathrm{mg\,L^{-1}}$. The confidence bounds correspond to a 95 % confidence interval, computed by bootstrapping ($N = 10^4$). The best fit curve is a generalized least squares model with a logit link function, yielding $R^2 = 0.54$ and was constrained to pass through the origin. The dependent variable was binarized before fitting the model, as polyp mortality can be seen as an effect on the organism.

Based on the analysis shown in Fig 5, categories of exposure have been chosen with limits corresponding to LC5 and LC25:

- Non-exposed and lowest exposed corals: $C \leq 1.25\,\mathrm{mg\,L^{-1}}$
- Intermediate exposed corals: $1.25\,\mathrm{mg\,L^{-1}} < C \leq 2.30\,\mathrm{mg\,L^{-1}}$
- Highest exposed corals: $C > 2.30\,\mathrm{mg\,L^{-1}}$

What we here refer to as low, intermediate and high doses, is based on the doses used in the toxicity test to ensure mortality was obtained, and does not refer to what we consider as low, medium, and high concentrations in situ and associated with, e.g., oil spills.

As such, the doses of 2-methylnaphthalene chosen in this study were not primarily chosen to be environmentally relevant. Compared to measured doses of naphthalenes in sea water samples during oil spills, e.g. Deepwater Horizon, the doses used in the present study are considerably higher [40]. Water samples collected and analyzed for oil compounds, including naphthalenes, during or shortly after an oil spill, are generally below the lowest levels of exposure reported in this study. In a study by Guyormach et al. [41], dissolved PAH concentration was monitored during a field trial in the North Sea, with 2 slicks of respectively $1\,\mathrm{m^3}$ and $3\,\mathrm{m^3}$ of Grane crude oil. The maximum concentration, for the sum of 1-methylnaphthalene and 2-methylnaphthalene, was below $2\,\mathrm{\mu g\,L^{-1}}$.

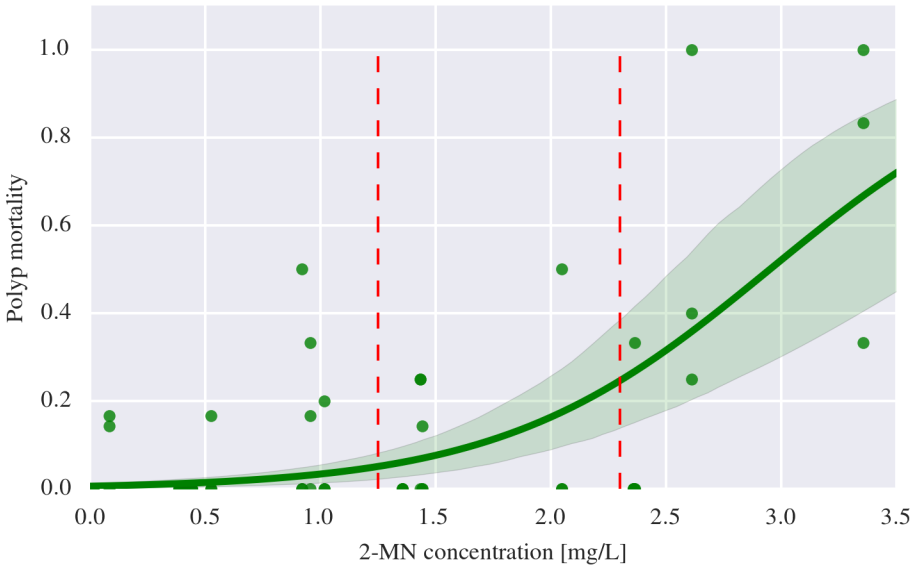

Fig 5. Dose-response curve for 2-methylnaphthalene exposure and polyp mortality ($n = 60$). The regression line with a 95 % confidence interval indicates that there is indeed a positive correlation between polyp mortality and 2-methylnaphthalene exposure. Some data points have similar values, and hence, overlap in the plot. The vertical red dashed lines indicate the 2-methylnaphthalene category thresholds and coincide with the 5 % and 25 % mortality levels (LC5 and LC25, respectively). The corresponding 2-methylnaphthalene concentrations are 1.25 mg L^{-1} and 2.3 mg L^{-1}, respectively.

PLS model

For the PLS model, a total of 10 latent variables were retained; cross-validation suggested an essentially flat plateau of model performance for 5 to 20 latent variables. The first six **X** loading vectors are shown in Fig 6 and Fig 7, for white and orange corals, respectively. The figures indicate which parts of the spectrum is important for explaining covariance between spectra and 2-methylnaphthalene concentration and polyp mortality. Several spectral features, i.e., peaks and dips, can be observed across the spectrum, especially for higher order loadings. Loading 5 and 6 exhibit high frequency noise, indicating that one is approaching an appropriate cutoff in number of latent variables. Some features appear to be present in both color morphs (e.g., the peak/dip at 650 nm for loading 5 in both color morphs), whereas others are observed only in one color morph (e.g., for white corals, a dip is observed in loading 3 at 540 nm, but no such dip is observed for orange corals). Each spectral dip or peak (note that the sign of loading vectors is arbitrary) can potentially be interpreted as absorption by a chemical compound in the coral. It is of interest to examine further the sources of these spectral features, as it would enable the creation of more robust interpretation models for hyperspectral imagery.

After fitting the PLS model to training data, **X** scores were extracted. The scores correspond to coordinates in the latent variable space. The first three score components for white coral data can be seen in Fig 8. One dot in the scatter plot corresponds to one coral spectrum, i.e., one hyperspectral image pixel. While the color scale in the figures is continuous, only 20 distinct values appear. This is due to the experimental setups, where each of the five treatment groups consisted of four replicates, giving a total of 20 exposure beakers containing 3 coral samples each. Measurements of

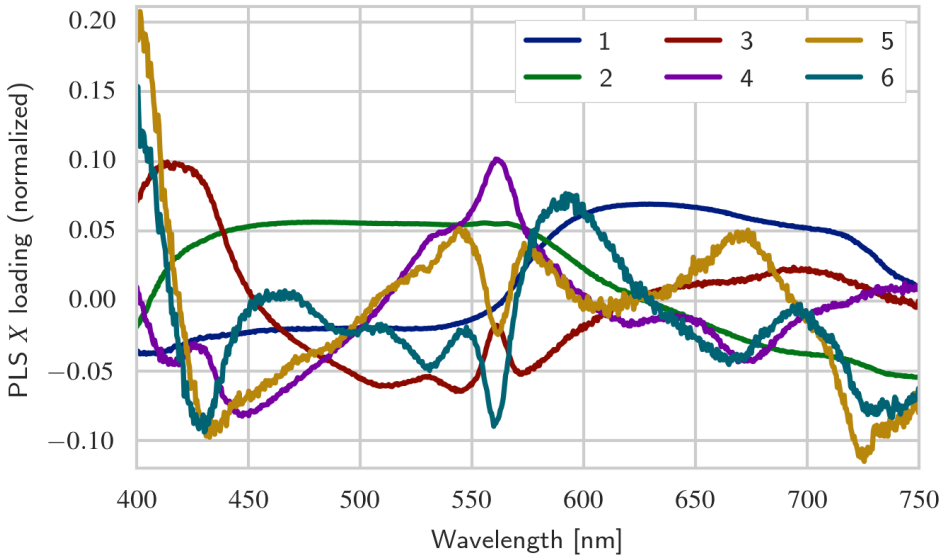

Fig 6. PLS X loadings for white corals. The PLS **X** loadings show which parts of the spectrum are significant in explaining covariance between spectra and 2-methylnaphthalene concentration and polyp mortality. Higher order loadings carry less significance in explaining the variation in the corals exposure doses and mortality; this is a property of the PLS algorithm.

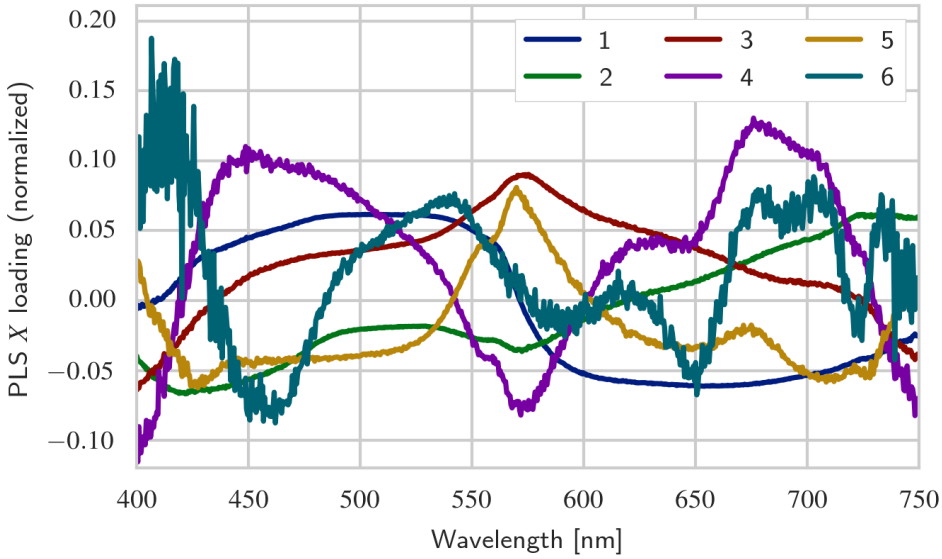

Fig 7. PLS X loadings for orange corals. Same as Fig 6, but created using data from orange corals. A notable difference is the significant noise in loading 6, indicating that explanatory power is decreasing at this point.

2-methylnaphthalene concentration were done for each replicate.

When examining Fig 8, we observe clustering of low exposure values near the origin,

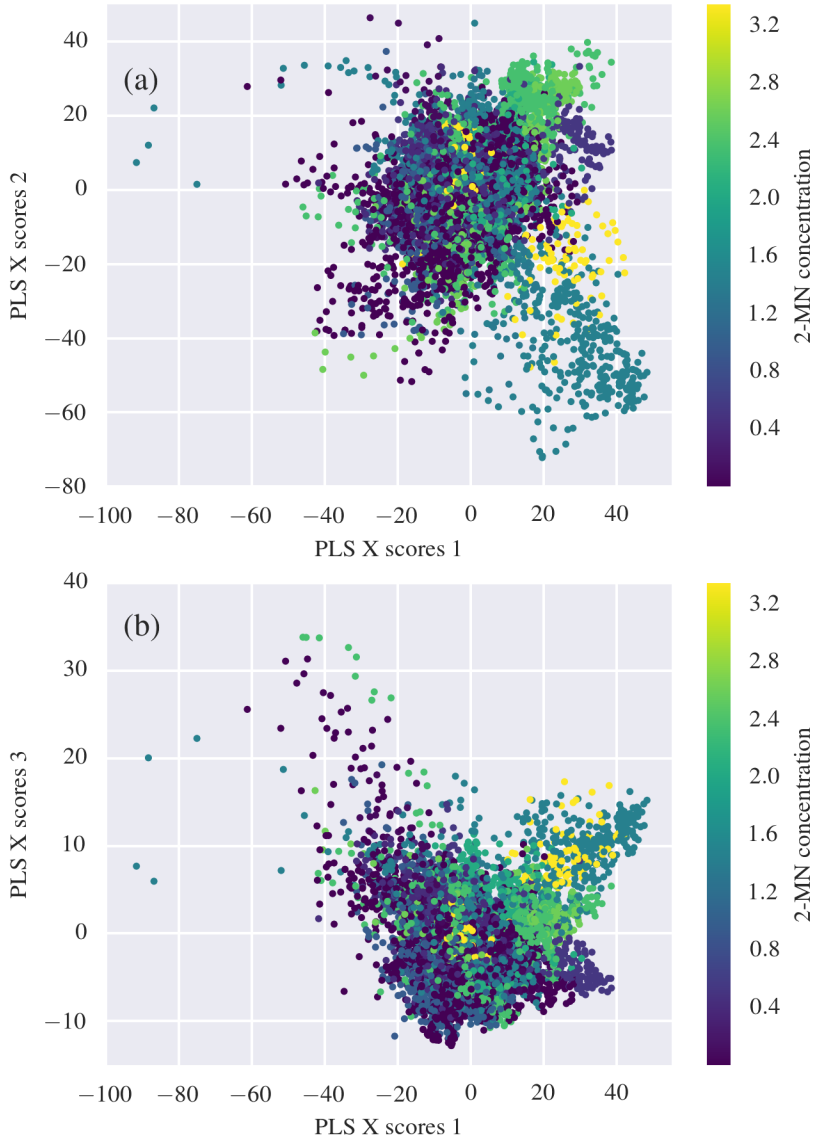

Fig 8. PLS scores for white corals. (a) shows scores for **X** latent variable 1 vs latent variable 2, (b) shows scores for **X** latent variable 1 vs latent variable 3. One dot corresponds to one spectrum (i.e. one hyperspectral image pixel) taken from a coral.

whereas spectra from corals exposed to higher values of 2-methylnaphthalene form scattered clusters outside of the central cluster. We attribute this clustering partly to the 2-methylnaphthalene exposure levels being highly clustered. When rotated in a 3-dimensional view, one can more easily see that the spectra of high exposed corals form a "shell" outside of the central cluster consisting mainly of low exposed corals, and do

not a simple linear structure. With this in mind, we note that a linear discriminant will not be able to separate the spectra from the lowest and highest concentrations, nor will a linear regression algorithm (including PLS regression) satisfactorily predict 2-methylnaphthalene exposure level. However, as we observe good separation between the non-exposed to lowest exposed corals, the intermediately exposed corals and the highest exposed corals, we have performed spectral classification using the nonlinear classification algorithm SVM.

Score plots analogous to Fig 8, but for orange *L. pertusa*, are given in S2 Figure: PLS **X** scores for orange corals. Finally, identical score plots but with polyp mortality as the color variable are shown for both color morphs in S3 Figure: PLS **X** scores for orange corals with mortality coloring.

Classification

The quality of the classification of exposure category is assessed using the metrics *precision*, P, and *recall*, R, which are frequently used in the context of classification. The metrics are defined as

$$P = \frac{T_p}{T_p + F_p} \tag{8}$$

and

$$R = \frac{T_p}{T_p + F_n}. \tag{9}$$

Here, T_p is the fraction of true positive classifications, and F_p and F_n is the fraction of false positive and false negative classification, respectively. Finally, we give the $F1$-score, which takes both precision and recall into account as the *harmonic* average:

$$F1 = 2\frac{PR}{P + R}. \tag{10}$$

Note that all quantities T_p, F_n, F_p, P, R, and $F1$ are defined on the interval $[0, 1]$, and that a high score of P, R, and $F1$ equal to 1 is optimal.

The input data is split $80 - 20$ into a training data set (80 %) and a test data set (20 %). The split is performed using random stratified sampling, giving each class (no or low, medium, and high exposure) a number of training data samples proportional to the size of the class. The classification model is fit to the training data set, and all classification results shown below are for the test data set.

Results for the three-class case are given in Table 3. The overall picture is that an accuracy in the range 78 % to 97 % is achieved using SVM classification. The poorest performance is found for high exposed corals. This is possibly due to the fact that fewer spectra were collected for these classes (see the "pixels" column of Table 3).

Per-organism classification

Obviously, each pixel of each coral cannot have its exposure level be classified separately. Hence, following classification of spectra, i.e., hyperspectral image pixels, we classify the corals at the *sample* level. This is done by the majority vote algorithm: the coral sample is of the exposure category that most of its pixels are. In this manner, spatial information is used to improve classification, without resorting to advanced image processing algorithms. When this is done, 100 % of all samples are classified in the correct exposure category.

An illustration of this final classification step is shown in Fig 9. Here, images of two corals for each of the three exposure categories are shown, with classified pixels shown

Table 3. Summary of classification results for single spectra, using the processing pipeline shown in Fig 4.

Color morph	Exposure	Pixels	P	R	F
White	Low	1252	0.87	0.95	0.91
	Medium	457	0.87	0.80	0.83
	High	440	0.92	0.78	0.84
	Total/avg	2149	0.88	0.88	0.88
Orange	Low	512	0.85	0.98	0.91
	Medium	235	0.94	0.79	0.86
	High	216	0.97	0.78	0.86
	Total/avg	963	0.90	0.89	0.89

Classification results for the three-class case. An overall $F1$ score of 0.88 and 0.89 is achieved for white and orange corals, respectively. The "pixels" column shows number of spectra collected for each class. Note that average values refer to the *harmonic* average.

in the row below. A few scattered pixels are classified incorrectly; e.g., in the center image, a few orange and black pixels are interspersed within the red pixels. By using the majority vote algorithm within each connected region, each *Lophelia pertusa* sample is classified correctly. This illustrates the power of spatial information when classifying hyperspectral images. Finally, we note that the spatial pattern below is valuable for environmental monitoring, as this technique can be used directly to generate maps of exposed corals.

Reference Alive corals

Finally, the 6 reference alive *L. pertusa* samples (2 orange and 4 white coral samples) that were in no way subjected to the handling and experimental conditions in the toxicity test, were scanned with the UHI. Classification on these corals were done with the SVM classifier model trained on data from the main treatment groups C0–C4.

The spectra taken from the orange reference corals classify with a precision of 1.00 and a recall of 0.95, whereas spectra from the white reference corals classify with a precision of 1.00 and a recall of 0.88. This is consistent with the classification results of single spectra in the results above, and gives a verification that the experimental conditions have not systematically modified the spectra, at least with respect to classification results.

Finally, at the organism level, 100 % of reference coral samples were classified in the category of nonexposed- or lowest exposed corals. This is correct, as the reference corals were kept separately from the coral samples exposed to 2-methylnaphthalene, and should thus be representative of healthy corals in the wild.

Conclusion

Underwater hyperspectral imaging has been shown capable of classifying the cold water coral *L. pertusa* according to their individual exposure to the toxic petroleum compound 2-methylnaphthalene, when categorized according to lethal concentration levels LC5 and LC25 (5% and 25% mortality, respectively). A classification model consisting of projection to latent structures followed by a support vector machine classifier achieves a classification score of 73% to 100% correctness for single spectra. When exploiting the spatial information in the hyperspectral images, a full 100% of *L. pertusa* samples are

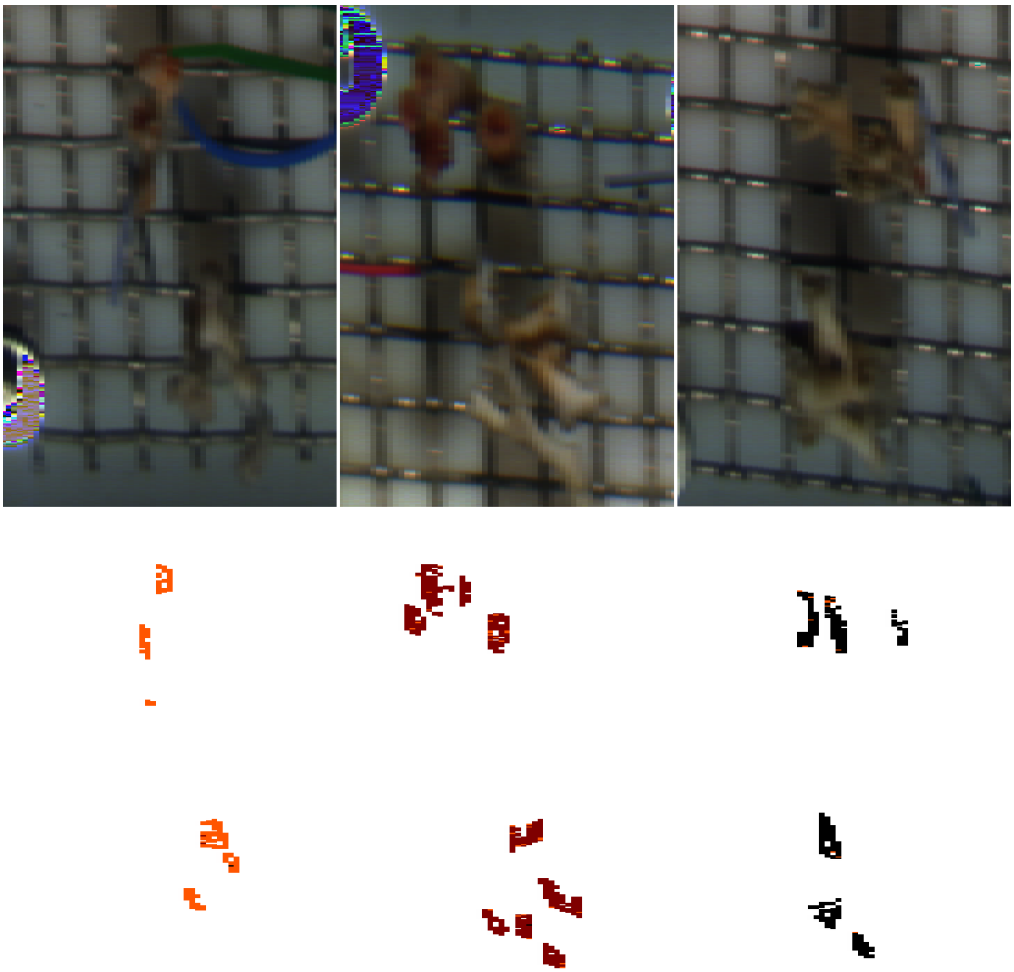

Fig 9. Classification of organisms. Two example corals from each exposure category: no- or low exposure (left), medium exposure (center), and high exposure (right). Note that the oddly colored patches in the lower left corner (left image) and upper left corner (center image) are caused by overexposure of a mechanical part holding the corals. The lower row shows classification into no- or low exposure (orange), medium exposure (red), and high exposure (right).

classified correctly under laboratory conditions. The model has been verified with hyperspectral images of reference coral samples not exposed to any toxic compound.

Future work

Scientists have often struggled to provide an integrated and non invasive assessment of coral health status. In that respect, this study represents the first step towards a non-invasive, automated method for in situ mapping of deep-water coral condition. In order to develop exposure mapping using underwater hyperspectral imaging into a field ready method, several challenges remain. Such a tool would be more valuable if several indicator species can be used, not just *L. pertusa*. Further studies should be conducted on environmentally relevant doses of relevant mixtures of toxicants, as these are encountered following oil spills. In a coral physiology perspective, future studies should

focus on assessing the underlying biochemical mechanisms for the mortality-linked spectral features, analogous to the widely discussed loss of colors (coral bleaching) caused by the death of symbiont chlorophyll containing algae of tropical corals. Determining whether coral mortality induced by other causes than toxicants, e.g., ocean acidification and smothering by drill cuttings, can be measured using the same hyperspectral technique may lend more generality to the method.

Supporting information

S1 Table: Measured 2-methylnaphthalene concentration in stock bottles and exposure beakers Table 4 shows the concentration of 2-methylnaphthalene measured in water samples collected from stock solutions every 24 h during the 96 h exposure period. The average (avg) value and corresponding standard deviation (std dev) are also given. Nominal concentrations, C_{nom}, are listed for each treatment group. Each water sample was performed in duplicate, with each duplicate labeled I or II in the table.

Table 5 shows the same results, but for the exposure beakers. The exposure was performed with 3 corals in each exposure beaker, across 4 replicates for each of the 5 treatment groups.

Regarding the analyses performed on the 2-MN water samples, the limit of quantification is $0.1\,\mathrm{mg\,L^{-1}}$, and the uncertainty is 20 % at the limit of quantification. This uncertainty decreases above the limit of quantification. Additional uncertainty is expected as the magnetic stirring mechanism cannot operate at high frequency, as this would disturb the coral samples.

Table 4. Measured 2-methylnaphthalene concentration ($\mathrm{mg\,L^{-1}}$) in stock bottles

TG	C0			C1			C2			C3			C4		
C_{nom}	0.00			1.03			2.27			5.00			8.00		
Time (h)	I	II	avg	I	II	avg	I	II	avg	I	II	avg	I	II	avg
0	0.0	0.0	0.0	1.4	1.3	1.3	3.2	3.2	3.2	3.0	3.0	3.0	7.9		7.9
24	0.0	0.0	0.0	1.5	1.5	1.5	2.9	2.8	2.8	1.8	1.8	1.8	7.8	8.2	8.0
48	0.0	0.0	0.0	1.3	1.3	1.3	2.4	2.5	2.4	5.0	4.4	4.7	10.2	7.3	8.8
72	0.0	0.0	0.0	1.1	1.0	1.1	2.1	1.9	2.0	4.7	4.3	4.5	7.4	6.1	6.7
avg	0.0	0.0	0.0	1.3	1.3	1.3	2.6	2.6	2.6	3.6	3.4	3.5	8.3	7.2	7.9
std dev	0.0	0.0	0.0	0.2	0.2	0.2	0.5	0.6	0.5	1.5	1.3	1.4	1.3	1.1	0.8
% of nominal						125			115			70			98

The bottom three rows indicate average, standard deviation, and percentage of nominal concentration for each column, respectively. The missing value in column C4 II was not analyzed.

Table 5. Measured 2-methylnaphthalene concentration ($\mathrm{mg\,L^{-1}}$) in exposure beakers

Treatment group		C0			C1			C2			C3			C4		
C_{nom}		0.00			1.03			2.27			5.00			8.00		
Time (h)	Replicate	I	II	avg	I	II	avg	I	II	avg	I	II	avg	I	II	avg
0	R1	0.0	0.0	0.0	0.0	0.0	0.0	0.4	0.4	0.4	0.4	0.4	0.4	1.1	1.0	1.1
	R2	0.0	0.0	0.0	0.1	0.1	0.1	0.4	0.4	0.4	0.0	0.0	0.0	0.0	0.0	0.0
	R3	0.0	0.0	0.0	0.1	0.1	0.1	0.0	0.0	0.0	0.4	0.4	0.4	1.0	1.0	1.0
	R4	0.1	0.0	0.0	0.1	0.1	0.1	0.0	0.0	0.0	0.4	0.4	0.4	0.0	0.0	0.0
24	R1	0.0	0.0	0.0	0.4	0.4	0.4	1.9	2.0	2.0	1.1	1.3	1.2	2.0	2.5	2.2
	R2	0.0	0.0	0.0	0.4	0.4	0.4	0.9	1.1	1.0	0.0	0.0	0.0	2.2	2.8	2.5
	R3	0.0	0.0	0.0	0.4	0.5	0.5	1.2	1.4	1.3	0.6	1.4	1.0	3.2	3.8	3.5
	R4	0.0	0.0	0.0		0.8	0.8	1.1	1.1	1.1	0.7	1.4	1.1	1.6	2.6	2.1
48	R1	0.0	0.0	0.0	0.6	0.6	0.6	1.8	1.9	1.9	2.0	2.0	2.0	3.3	3.9	3.6
	R2	0.0	0.0	0.0	0.6	0.7	0.6	1.2	1.3	1.3	0.5	0.0	0.3	3.4	3.9	3.7
	R3	0.0	0.0	0.0	0.7	0.7	0.7	1.4	1.5	1.5	2.7	2.0	2.3	4.1	4.9	4.5
	R4	0.0	0.0	0.0	0.7	0.7	0.7	1.3	1.4	1.3	1.3	2.1	1.7	2.6	3.2	2.9
72	R1	0.0	0.0	0.0	0.6	0.6	0.6	1.2	1.3	1.2	2.1	2.3	2.2	3.2	3.9	3.5
	R2	0.0	0.0	0.0	0.6	0.7	0.6	1.1	1.2	1.2	0.0	0.0	0.0	2.3	4.2	3.3
	R3	0.0	0.0	0.0	0.3	0.3	0.3	1.3	1.4	1.3	8.9	2.4	5.7	4.2	4.6	4.4
	R4	0.0	0.0	0.0	0.6	0.7	0.7	1.2	1.4	1.3	2.7	2.4	2.6	3.0	3.5	3.2
avg		0.0	0.0	0.0	0.4	0.5	0.5	1.0	1.1	1.1	1.5	1.2	1.3	2.3	2.9	2.6
std dev		0.0	0.0	0.0	0.2	0.3	0.3	0.6	0.6	0.6	2.2	1.0	1.5	1.3	1.6	1.4
% of nominal							44			47			27			32

The bottom three rows indicate average, standard deviation, and percentage of nominal concentration for each column, respectively.

S2 Figure: PLS X scores for orange corals PLS **X** scores for orange corals are given here. The results correspond exactly to those presented in Fig 8, except that the figure below presents results for the white color morph.

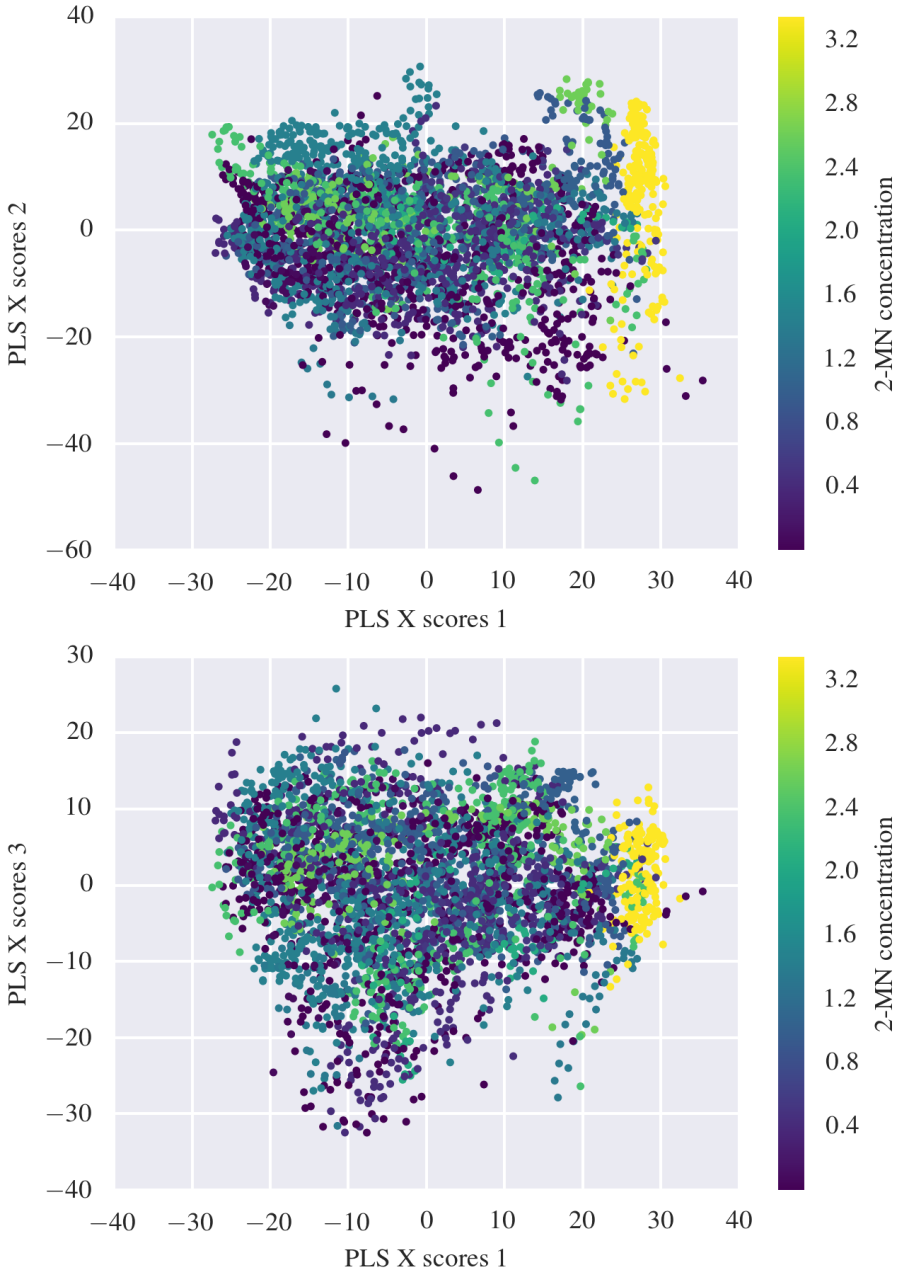

Fig 10. PLS X scores for spectra from orange corals.

S3 Figure: PLS X scores for orange corals with mortality coloring PLS **X** scores colored with the mortality variable. The results correspond exactly to those presented in Fig 8 and 10, except for the coloring of the dots.

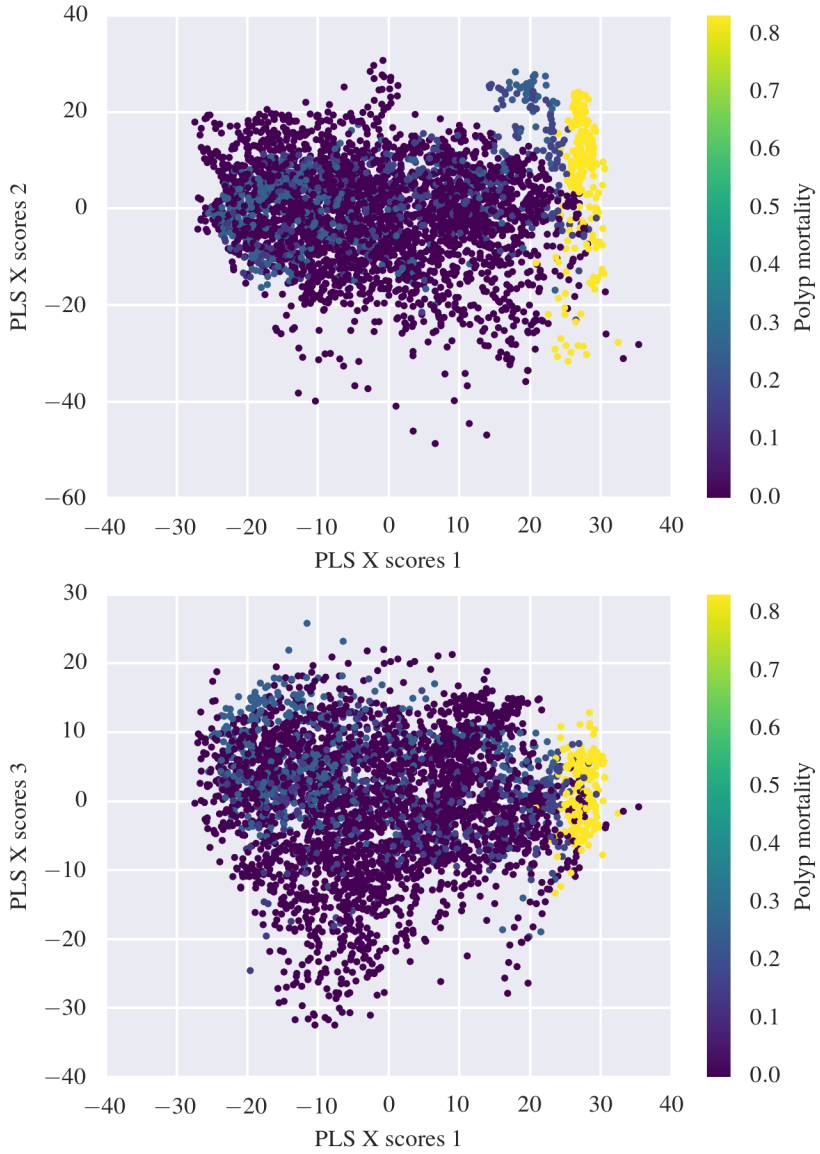

Fig 11. PLS X scores for spectra from orange corals. The color map indicates the polyp mortality.

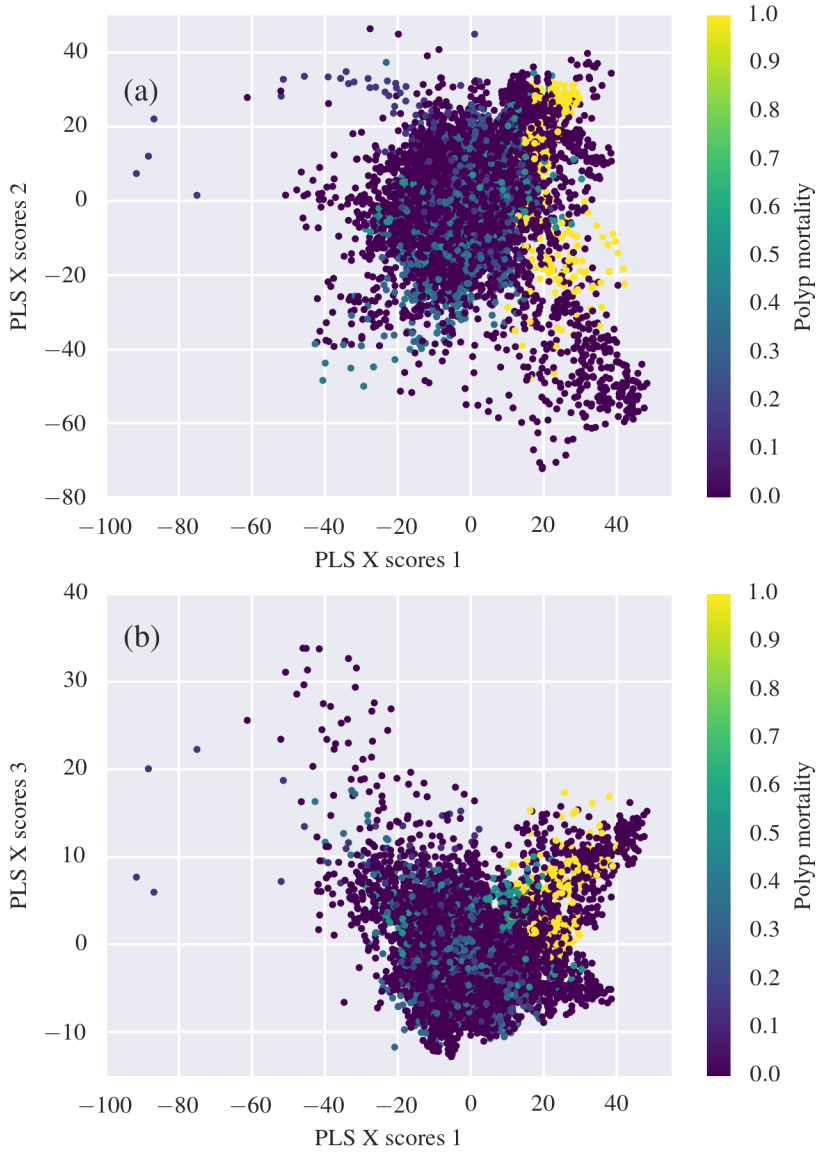

Fig 12. PLS X scores for spectra from white corals. The color map indicates the polyp mortality.

Acknowledgements

This study is part of the joint industry project "New technology and methods for mapping and monitoring of seabed habitats", financed by the Research Council of Norway (RCN), Statoil, ConocoPhillips Skandinavia, Dea Norge, ENI Norge, Lundin Norway, Total E&P Norge, Norwegian Deepwater Programme, Ecotone, and Akvaplan-niva (RCN project number 235440/E30).

The exposure experiment recieved financial support from the project "Species Sensitivity Distribution for Deep Sea Species and Toxicity of continuous and spiked exposures to crude oil at 1 atm for deep sea species", led by Akvaplan-niva and financed by the American Petroleum Institute (API).

The authors thank the captain and crew of R/V Gunnerus for collection of coral samples and Johanna Järnegren at the Norwegian Institute for Nature Research (NINA) for advice on coral sampling.

Advice from Geir Johnsen at the Norwegian University of Science and Technology (NTNU) on set-up of the hyperspectral imager rig is highly appreciated.

The personnel at Akvaplan-niva Research and Innovation Station Kraknes (RISK) are acknowledged for facilitating the experiments.

The authors thank Ingvild Andersson at NTNU for valuable discussions on the hyperspectral data results.

References

1. Liu G, Strong AE, Skirving W, Arzayus LF. Overview of NOAA coral reef watch program's near-real time satellite global coral bleaching monitoring activities. In: Proceedings of the 10th International Coral Reef Symposium. June; 2006. p. 1783–1793.

2. Roberts JM, Wheeler AJ, Freiwald A. Reefs of the Deep: The Biology and Geology of Cold-Water Coral Ecosystems. Science. 2006;312(5773):543–547. doi:10.1126/science.1119861.

3. Fosså JH, Mortensen P, Furevik DM. The deep-water coral Lophelia pertusa in Norwegian waters: distribution and fishery impacts. Hydrobiologia. 2002;471(1):1–12. doi:10.1023/A:1016504430684.

4. Cairns SD. Scleractinia of the temperate North Pacific. Smithson Contrib Zool. 1994;(557):1–150.

5. Upadhyay RR, Liaaen-Jensen S. Animal carotenoids. 5. The carotenoids of some Anthozoa. Acta chemica Scandinavica. 1970;24(8):3055–3057.

6. Elde AC, Pettersen R, Bruheim P, Järnegren J, Johnsen G. Pigmentation and spectral absorbance signatures in deep-water corals from the Trondheimsfjord, Norway. Marine drugs. 2012;10(6):1400–1411. doi:10.3390/md10061400.

7. Mortensen PB, Hovland M, Brattegard T, Farestveit R. Deep water bioherms of the scleractinian coral Lophelia pertusa (L.) at 64° N on the Norwegian shelf: Structure and associated megafauna. Sarsia. 1995;80(2):145–158. doi:10.1080/00364827.1995.10413586.

8. Costello MJ, McCrea M, Freiwald A, Lundälv T, Jonsson L, Bett BJ, et al. Role of cold-water Lophelia pertusa coral reefs as fish habitat in the NE Atlantic. In: Cold-water corals and ecosystems. Berlin, Heidelberg: Springer; 2005. p. 771–805. Available from: `http://dx.doi.org/10.1007/3-540-27673-4_41`.

9. Freiwald A. Geobiology of Lophelia pertusa (Scleractinia) reefs in the North Atlantic. Habilitation thesis, the University of Bremen; 1998.

10. Bellwood DR, Hughes TP, Folke C, Nyström M. Confronting the coral reef crisis. Nature. 2004;429(6994):827–833. doi:10.1038/nature02691.

11. Albright R, Caldeira L, Hosfelt J, Kwiatkowski L, Maclaren JK, Mason BM, et al. Reversal of ocean acidification enhances net coral reef calcification. Nature. 2016;531(7594):362–365. doi:10.1038/nature17155.

12. Barott K, Smith J, Dinsdale E, Hatay M, Sandin S, Rohwer F. Hyperspectral and physiological analyses of coral-algal interactions. PloS one. 2009;4(11):e8043. doi:10.1371/journal.pone.0008043.

13. Turley C, Roberts J, Guinotte J. Corals in deep-water: will the unseen hand of ocean acidification destroy cold-water ecosystems? Coral reefs. 2007;26(3):445–448. doi:10.1007/s00338-007-0247-5.

14. Maier C, Hegeman J, Weinbauer M, Gattuso JP. Calcification of the cold-water coral Lophelia pertusa, under ambient and reduced pH. Biogeosciences. 2009;6(8):1671–1680. doi:10.5194/bg-6-1671-2009.

15. Rogers AD. The Biology of Lophelia pertusa (Linnaeus 1758) and Other Deep-Water Reef-Forming Corals and Impacts from Human Activities. International review of hydrobiology. 1999;84(4):315–406. doi:10.1002/iroh.199900032.

16. Larsson AI, van Oevelen D, Purser A, Thomsen L. Tolerance to long-term exposure of suspended benthic sediments and drill cuttings in the cold-water coral Lophelia pertusa. Marine pollution bulletin. 2013;70(1):176–188. doi:10.1016/j.marpolbul.2013.02.033.

17. White HK, Hsing PY, Cho W, Shank TM, Cordes EE, Quattrini AM, et al. Impact of the Deepwater Horizon oil spill on a deep-water coral community in the Gulf of Mexico. Proceedings of the National Academy of Sciences. 2012;109(50):20303–20308. doi:10.1073/pnas.1118029109.

18. Beyer J, Trannum HC, Bakke T, Hodson PV, Collier TK. Environmental effects of the Deepwater Horizon oil spill: a review. Marine Pollution Bulletin. 2016;110(1):28–51. doi:10.1016/j.marpolbul.2016.06.027.

19. Joyce KE, Phinn SR. Hyperspectral analysis of chlorophyll content and photosynthetic capacity of coral reef substrates. Limnology and Oceanography. 2003;48(1part2):489–496. doi:10.4319/lo.2003.48.1_part_2.0489.

20. Kutser T, Miller I, Jupp DLB. Mapping coral reef benthic substrates using hyperspectral space-borne images and spectral libraries. Estuarine, Coastal and Shelf Science. 2006;70(3):449 – 460. doi:http://doi.org/10.1016/j.ecss.2006.06.026.

21. Mumby PJ, Skirving W, Strong AE, Hardy JT, LeDrew EF, Hochberg EJ, et al. Remote sensing of coral reefs and their physical environment. Marine pollution bulletin. 2004;48(3):219–228. doi:10.1016/j.marpolbul.2003.10.031.

22. Holden H, LeDrew E. Hyperspectral identification of coral reef features. International Journal of Remote Sensing. 1999;20(13):2545–2563. doi:10.1080/014311699211921.

23. Gleason A, Reid R, Voss K. Automated classification of underwater multispectral imagery for coral reef monitoring. In: OCEANS 2007. IEEE; 2007. p. 1–8. Available from: `http://dx.doi.org/10.1109/OCEANS.2007.4449394`.

24. Chennu A, Färber P, Volkenborn N, Al-Najjar MA, Janssen F, De Beer D, et al. Hyperspectral imaging of the microscale distribution and dynamics of microphytobenthos in intertidal sediments. Limnology and Oceanography: Methods. 2013;11(10):511–528. doi:10.4319/lom.2013.11.511.

25. Johnsen G, Ludvigsen M, Sørensen A, Aas LMS. The use of underwater hyperspectral imaging deployed on remotely operated vehicles-methods and applications. IFAC-PapersOnLine. 2016;49(23):476–481. doi:10.1016/j.ifacol.2016.10.451.

26. Johnsen G, Volent Z, Dierssen H, Pettersen R, Ardelan M, Søreide F, et al. Underwater hyperspectral imagery to create biogeochemical maps of seafloor properties. In: Watson J, Zielinski O, editors. Subsea optics and imaging. Cambridge: Woodhead Publishing Ltd.; 2013. p. 508–535.

27. Johnsen G. Underwater hyperspectral imaging. 2013;US patent US8767205 B2.

28. Pope RM, Fry ES. Absorption spectrum (380–700 nm) of pure water. II. Integrating cavity measurements. Appl Opt. 1997;36(33):8710–8723. doi:10.1364/AO.36.008710.

29. Tollefson J. Computers on the reef. Nature. 2016;537:123–124. doi:10.1038/537123a.

30. Eide I, Westad F, Nilssen I, de Freitas FS, dos Santos NG, dos Santos F, et al. Integrated environmental monitoring and multivariate data analysis—A case study. Integrated Environmental Assessment and Management. 2017;13(2):387–395. doi:10.1002/ieam.1840.

31. Osterloff J, Nilssen I, Eide I, de Oliveira Figueiredo MA, de Souza Tâmega FT, Nattkemper TW. Computational visual stress level analysis of calcareous algae exposed to sedimentation. PloS one. 2016;11(6):e0157329. doi:10.1371/journal.pone.0157329.

32. Brooke S, Järnegren J. Reproductive periodicity of the scleractinian coral Lophelia pertusa from the Trondheim Fjord, Norway. Marine Biology. 2013;160(1):139–153. doi:10.1007/s00227-012-2071-x.

33. Butler JD, Parkerton TF, Letinski DJ, Bragin GE, Lampi MA, Cooper KR. A novel passive dosing system for determining the toxicity of phenanthrene to early life stages of zebrafish. Science of the Total Environment. 2013;463:952–958. doi:10.1016/j.scitotenv.2013.06.079.

34. Wold S, Sjöström M, Eriksson L. PLS-regression: a basic tool of chemometrics. Chemometrics and intelligent laboratory systems. 2001;58(2):109–130. doi:10.1016/S0169-7439(01)00155-1.

35. Pedregosa F, Varoquaux G, Gramfort A, Michel V, Thirion B, Grisel O, et al. Scikit-learn: Machine Learning in Python. Journal of Machine Learning Research. 2011;12:2825–2830.

36. Wu TF, Lin CJ, Weng RC. Probability estimates for multi-class classification by pairwise coupling. Journal of Machine Learning Research. 2004;5:975–1005.

37. López M, Górriz JM, Ramírez J, Salas-Gonzalez D, Chaves R, Gómez-Río M. SVM with Bounds of Confidence and PLS for Quantifying the Effects of Acupuncture on Migraine Patients. In: Corchado E, Kurzyński M, Woźniak M, editors. Hybrid Artificial Intelligent Systems: 6th International Conference, HAIS 2011, Wroclaw, Poland, May 23-25, 2011, Proceedings, Part I. Berlin, Heidelberg: Springer Berlin Heidelberg; 2011. p. 132–139. Available from: http://dx.doi.org/10.1007/978-3-642-21219-2_18.

38. Kohavi R. A Study of Cross-validation and Bootstrap for Accuracy Estimation and Model Selection. In: Proceedings of the 14th International Joint Conference on Artificial Intelligence - Volume 2. IJCAI'95. San Francisco, CA, USA: Morgan Kaufmann Publishers Inc.; 1995. p. 1137–1143. Available from: http://dl.acm.org/citation.cfm?id=1643031.1643047.

39. Shelton G. Lophelia pertusa (L.): electrical conduction and behaviour in a deep-water coral. Journal of the Marine Biological Association of the United Kingdom. 1980;60(02):517–528. doi:10.1017/S0025315400028538.

40. Reddy CM, Arey JS, Seewald JS, Sylva SP, Lemkau KL, Nelson RK, et al. Composition and fate of gas and oil released to the water column during the Deepwater Horizon oil spill. Proceedings of the National Academy of Sciences. 2012;109(50):20229–20234. doi:10.1073/pnas.1101242108.

41. Guyomarch J, Van Ganse S. Determination of polynuclear aromatic hydrocarbons in seawater following an experimental oil spill by Stir Bar Sorptive Extraction (SBSE) and thermal desorption GC-MS. In: Proceedings of the 33rd AMOP Technical Seminar on Environmental Contamination and Response. vol. 1; 2010. p. 181–187.